Towards Single Antenna Phase-Coherent INS-Beamforming to Enable RTK with Low-End Antennas

Jürgen Dampf, Mohamed Bochkati, Thomas Pany
Institute of Space Technology and Space Applications (ISTA), Space Systems Research Center (FZ-Space)
Universität der Bundeswehr München (UniBw M)

BIOGRAPHY

Dr. Jürgen Dampf works as a software development engineer at Rohde & Schwarz GmbH & Co. KG in the department for high-end spectrum analysis and as a research associate at the Universität der Bundeswehr München. He received his PhD in Navigation at the Graz University of Technology. Formerly he worked as a GNSS R&D engineer at Trimble Terrasat GmbH, as CTO at IGASPIN GmbH and as GNSS system engineer at IFEN GmbH. His research topics range from Bayesian direct position estimation, GNSS reflectometry, multi-sensor fusion and integrated navigation, synthetic antenna beamforming, efficient GNSS signal processing algorithms for desktop and embedded platforms and jamming/spoofing signal generation and mitigation techniques.

Mohamed Bochkati is a research associate at the Institute of Space Technology and Space Applications (ISTA) at the Universität der Bundeswehr München (UniBw M). His research focuses on Deeply Coupled GNSS/INS integration and novel calibration techniques for MEMS-IMUs. Before he joined the University of the Bundeswehr, he was a research associate at the Institute of Geodesy (ife) at the Leibniz University Hannover, where his research activities include quantum inertial navigation systems and GNSS receiver clock modeling. He holds a Bachelor's and Master's degree in Geodesy and Geoinformation from Technical University Munich.

Prof. Thomas Pany is with the Universität der Bundeswehr München (UniBw M) at Space Systems Research Center (FZ-Space) where he leads the satellite navigation unit LRT 9.2 of the Institute of Space Technology and Space Applications (ISTA). He teaches navigation focusing on GNSS, sensors fusion and aerospace applications. Within LRT 9.2 a good dozen of full-time researchers investigate GNSS system and signal design, GNSS transceivers and high-integrity multi-sensor navigation (inertial, LiDAR) and is also developing a modular UAV-based GNSS test bed. ISTA also develops the MuSNAT GNSS software receiver and recently focuses on smartphone positioning and GNSS/5G integration. He has a PhD from the Graz University of Technology (sub auspiciis) and worked in the GNSS industry for seven years. He authored around 200 publications including one monography and received five best presentation awards from the US Institute of Navigation. Thomas Pany also organizes the Munich Satellite Navigation Summit.

ABSTRACT

The sector of mass-market global navigation satellite system (GNSS) receivers experiences a continuous growth, and the demand for reliable and precise positioning becomes higher than ever, considering for example the increasing number of location based services (LBS) in smartphones or the field of autonomous driving (EUSPA, 2022). In these applications, size and shape of the antennas become subject to form-factor driven design, leading to degraded GNSS performance mainly caused by unfiltered multipath. Most GNSS receivers are already available loosely or tightly coupled with an inertial navigation system (INS) to improve the robustness and positioning performance, but precise positioning techniques like real-time kinematics (RTK) and Precise Point Positioning (PPP) still degrade when multipath is present. Nevertheless, a rarely investigated pure software based method, which is called synthetic aperture processing (SAP) or "Supercorrelation", is capable of purifying the GNSS observations from multipath on the tracking loop level. Thus, our overall target is the realization and evaluation of SAP in a newly developed MATLAB software receiver (MSRx) using both low and high-quality sensors, which unravels to three steps: At first, the implementation and analysis of an external Doppler-aided phase locked loop (PLL). Second, the realisation of an external carrier-range aiding of the PLL including co-operated (CO-OP)-tracking to estimate the receiver clock, and third, the increase of the coherent integration time, e.g. up to 1-2 seconds, to fully exploit the effect of SAP beamforming. The first step, i.e. the external Doppler-aided PLL, implicitly exploits the concept of SAP to a certain extent, when considering proper settings. Consequently, this stage can be seen as a simplest form of SAP. This work focuses on this rather trivial realization of SAP using an external Doppler aided PLL and discusses the achieved tracking performance and positioning results.

I. INTRODUCTION

GNSS has become an important backbone infrastructure for millions of users worldwide, thanks to its global availability, accuracy as well as the low cost of user equipment. This technology has become vital for many application fields, namely terrestrial, marine and airborne. However, some critical applications require enhanced performance and increased robustness to withstand different sources of signal disturbance, such as signal reflection, jamming or spoofing attacks that degrade the overall quality of the system solution or even render it unavailable for longer time spans. In case of mass-market applications, where strict limitations on the GNSS antenna are present, the conditions to achieve precise PPP or RTK position velocity and time (PVT) solutions become even more demanding. Previous publications, such as Sharma et al. (2021) precisely summarize the status quo. Low-cost set-ups, like in a smartphone, typically use an omni-directional linearly or elliptically polarized low gain antenna, which results in two major problems:

1. The antenna phase center (APC) is unknown and more variable compared to high-end antennas
2. The antenna has a poor multipath suppression

Both issues impact the positioning performance significantly, such that none or only few RTK fixed position solutions may be achieved even in open-sky conditions. The work in Sharma et al. (2021) made a very important step, as they managed to perform a phase center variation (PCV) calibration for a smartphone and furthermore achieved fixed solutions when placing the mobile phone on a choke-ring platform. The choke-ring platform aims to suppress the ground multipath, similar but more effective as a simple metal-made ground plate. Since the use of a choke-ring is of course unacceptable for mass-market applications, other means to reduce the multipath need to be found. SAP is an effective way to suppress multipath and improve the positioning performance. The realization of SAP as an integral part of a GNSS receiver or as a separate post-processing step would be possible in most cases, because most devices are already equipped with an inertial measurement unit (IMU) to deliver an integrated GNSS/INS solution and in addition a reasonably powerful embedded processor, e.g. a system-on-chip (SoC) architecture, is present in mobile phones. These ingredients allow for advanced post-correlation beamforming techniques based on antenna motion trajectories, as e.g. proposed in Pany et al. (2013); Dampf et al. (2016, 2017). Several examples in literature exist, such as in Faragher et al. (2018), that prove that these SAP algorithms can be moved onto embedded systems. This method relies on the principle that the multipath will always have a different phase signature than the line-of-sight signal, thus an INS is mandatory for this realisation. Generally speaking, two main approaches for SAP exist:

1. The realization using an external Doppler-aided PLL and
2. The realization using an external carrier-range aiding of the PLL.

For both cases the receiver clock error could be estimated with the so-called CO-OP tracking (Gao and Lachapelle, 2008) to be able to fully minimize the PLL bandwidth.

Traditionally, IMU are used to perform this task, since they are able to provide information about position, velocity and orientation with higher update rates, i.e. up to 2KHz, and therefore can capture the movement of the the hosted platform in challenging dynamic environments. A simple tight-coupling GNSS/INS receiver with external high-quality Doppler-aiding (Spilker Jr. et al., 1996) is very common. In Alban et al. (2003) and in Gebre-Egziabher et al. (2005) it has been shown that coupling the IMU on the tracking loop level is most beneficial in terms of robustness by narrowing the noise bandwidth of the carrier-tracking loop using an external estimate of the of the Doppler shift of the GPS signal. Both contributions highlighted the role of the quality of both components, the employed IMU sensors and the receiver internal oscillator. There is a significant difference in the quality of the external Doppler information if low-cost micro-electro-mechanical systems (MEMS) IMUs are coupled with a receiver that hosts a temperatur controlled crystal oscillator (TCXO) comparing to improvements achieved by using a navigation-grade IMU and a oven controlled crystal oscillator (OCXO). This means, besides reducing the dynamic by using the Doppler derived from the IMU measurement, the clock error should also be estimated or tracked to remove the oscillator's g-sensitivity from the carrier discriminator output, so that only additive white Gaussian noise (AWGN) remains in these components with narrower bandwidth. This was shown in both theoretical and simulation domain. A demonstration of this technique was also given by Tsujii et al. (2011) for a flight test. There, the analyses during aircraft take-off showed that the noise bandwidth of the tracking loop could be reduced to three Hertz by external aiding. Also, Doppler aiding by a low-cost MEMS INS showed a similar performance compared to Doppler aiding by a navigation grade INS. Additionally, Zhang et al. (2017) shows an improved design of a MEMS INS-aided PLL under high dynamic circumstances to eliminate the impact of a step change due to a sudden jerk.

In this publication we report our progress towards the realization of SAP, which started by implementing and validating a MATLAB software-receiver (MSRx) based on sufficient statistics data (Bochkati et al., 2022) to speed up the implementation of new tracking algorithms. The current status discusses the realized Doppler-aided PLL in the context of SAP, whereas, as stated before, similar results as in literature were achieved. The innovative differentiation to existing publications regarding SAP will be the realization of an external high-quality RTK/INS Doppler and carrier-range aiding.

The remainder of this paper is organized as follows. In the next section, we give a brief overview of the structure of the developed MATLAB-based GNSS receiver (MSRx) with the new capability of accepting external high-quality Doppler-aiding information. After that we shed some light on the mathematical model used to compute and integrate the Doppler aiding within the MSRx on the tracking loop level, i.e. the PLL. Section IV discusses the achieved results with the realized Doppler-aided PLL in conjunction

with a high-rate MEMS IMU and compares them to a standard PLL. Chapter V addresses the Doppler-aided PLL in context of SAP, as it is the simplest realization of SAP. And finally in section VI, we describe briefly the way forward of realising the concept of SAP with an carrier-pseudorange aided PLL as well as the beamforming step as integral part of the tracking loop.

II. ARCHITECTURE OF THE MATLAB-BASED GNSS RECEIVER (MSRX)

The MSRx receiver was introduced for the first time in Bochkati et al. (2022), where the concept validation of the so-called sufficient statistics (Kay, 1993) to compress GNSS signal information in multi-correlator values, which allows the interpolation of the correlator number without any loss of information, has been explained and validated with real satellite signals. Generally speaking, our R&D framework for GNSS receiver development (incl. GNSS/INS integration) consists of two main steps: In the first step, a stable but less precise tracking algorithm is used, i.e. vector tracking (VT), to compute the sufficient statistics for a given scenario and the data is stored in files. In the second step, the receiver algorithm being assessed reads the sufficient statistics data from file and interpolates the actually needed early, prompt and late correlation values (or any other kind of GNSS data).

As outlined in Fig. 1, a GNSS software receiver MuSNAT (Pany et al., 2019) is switched to VT employing a vector delay lock loop (VDLL) and vector frequency lock loop (VFLL) and accepts a PVT solution at a user defined measurement rate (e.g. every 0.5 s) to control the numerically controlled oscillators (NCOs) for the next integration interval (Pany and Eissfeller, 2006). Every tracking channel activates a multi-correlator and the multi-correlator values are collected over the next measurement interval e.g. 0.5 s. All correlator values are time-tagged and the NCO values used for correlation are attached. Those batches of multi-correlator values are the sufficient statistics. They are produced for all tracked GNSS signals and are stored in files. Before employing the interpolated early, prompt and late correlation values for the tracking loops, we perform a navigation bits wipe-off operation (Kaplan and Hegarty, 2017) using the data archive of global positioning system (GPS) navigation messages as provided by Rothacher and Beyerle (2008). After that we switch from the Costas-loop discriminator to $atan2$ for the PLL discriminator and use longer coherent integration times, i.e. more than 20 ms.

Besides the sufficient statistics data, additional data like IMU measurements, navigation data for all satellites, PVT and atmospheric information is saved too. Based on the fact that the delivered data allows for a deep coupling (DC) GNSS/INS integration, the interface is called DC interface. A very simple MATLAB software receiver (MSRx) is operated on the data delivered by the DC interface. In comparison to the MSRx version showed in Bochkati et al. (2022), the receiver was extended to incorporate external high-quality aiding information such as Doppler which is computed by the commercial GNSS/INS software package from NovAtel (NovAtel Inc., 2018) in post-processing and afterwards fed back to the tracking loops to remove the existing vehicles dynamic considering the given bandwidth. In addition to that, the RTKLIB open-source GNSS software package (Suzuki and Kubo, 2014) was also included in the software tool-chain to process the generated observations, i.e. code- and carrier-phase, which provides various performance key parameters such accuracy or the achieved fixing-rates of the ambiguities.

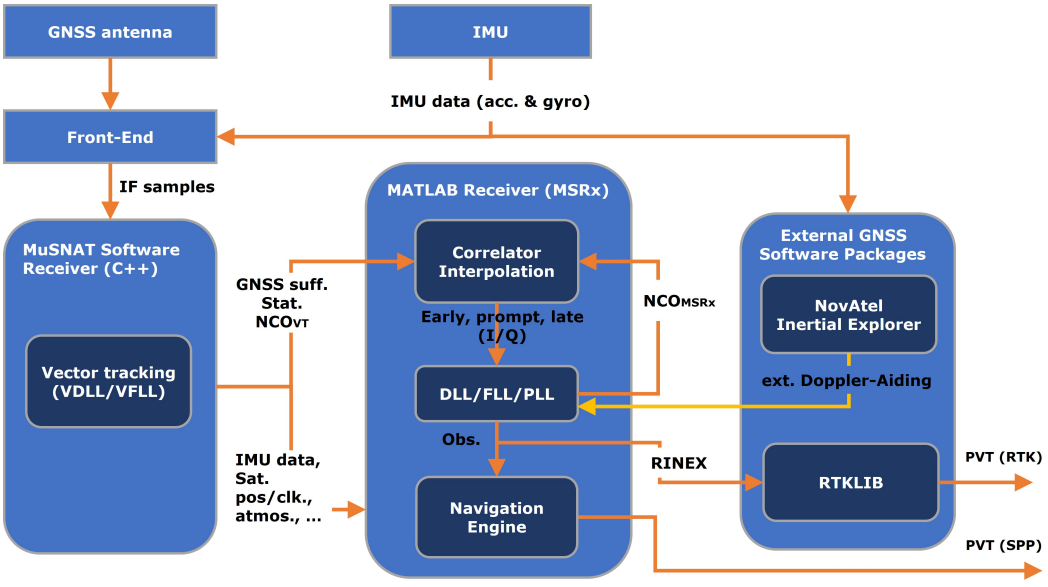

Figure 1: Block diagram and data flow for the MATLAB development framework. intermediate frequency (IF) samples and raw IMU data is pre-processed by a software receiver to generate the sufficient statistics on which a MATLAB software receiver (MSRx) is operated.

III. POST-PROCESSED DOPPLER-AIDING IN THE MSRX-RECEIVER

As depicted in the flowchart in Fig. 1, the external Doppler aiding is first derived from a tightly-coupled GNSS/INS coupling solution computed by the commercial GNSS/INS software package from NovAtel, which allows to have high-quality Doppler information. Thereafter, this data can be fed to the MSRx receiver to support the tracking loops, i.e. PLL or delay locked loop (DLL)/Frequency Locked Loop (FLL). The computed GNSS/INS solution can be used in turn as reference trajectory to asses the quality of the aided carrier tracking loops. For the sake of simplicity we are going to refer to the Doppler information as $f_{d,\text{INS}}$ instead of $f_{d,\text{GNSS/INS}}$. This nomenclature will also be used for any parameter related to this observation.

The Doppler frequency of the carrier signal can be expressed simply as the velocity of the receiver relative to the transmitter, projected onto the line-of-sight (LOS) vector. This relationship is expressed as follows

$$f_{d,\text{INS}} = \frac{1}{\lambda}\left(\mathbf{v}_{\text{INS}} - \mathbf{v}^S\right) \cdot \mathbf{l}^e \tag{1}$$

where λ is the wavelength, $\mathbf{v}_{\text{INS}}$ is the velocity of receiver antenna derived from the INS (considering the lever-arm between IMU and antenna phase center (APC)), $\mathbf{v}^S$ is the velocity of satellite and $\mathbf{1}^e$ represents a unit LOS vector from the APC to the satellite, which in turn incorporates both, the position derived from the inertial sensor and the satellite position expressed in the earth centered earth fixed (ECEF) coordinate frame,

$$\mathbf{l}^e = \begin{bmatrix} l_1 & l_2 & l_3 \end{bmatrix}^T = \begin{bmatrix} \frac{X_{\text{INS}} - X^S}{\rho} & \frac{Y_{\text{INS}} - Y^S}{\rho} & \frac{Z_{\text{INS}} - Z^S}{\rho} \end{bmatrix} \tag{2}$$

where ρ is the geometric range between satellite and INS

$$\rho = \sqrt{\left(X_{\text{INS}} - X^S\right)^2 + \left(Y_{\text{INS}} - Y^S\right)^2 + \left(Z_{\text{INS}} - Z^S\right)^2}. \tag{3}$$

In order to include the computed $f_{d,\text{INS}}$ into the carrier phase tracking procedure as described by the block diagram in Fig. 2, the second order loop filter can be used (Teunissen and Montenbruck, 2017) as

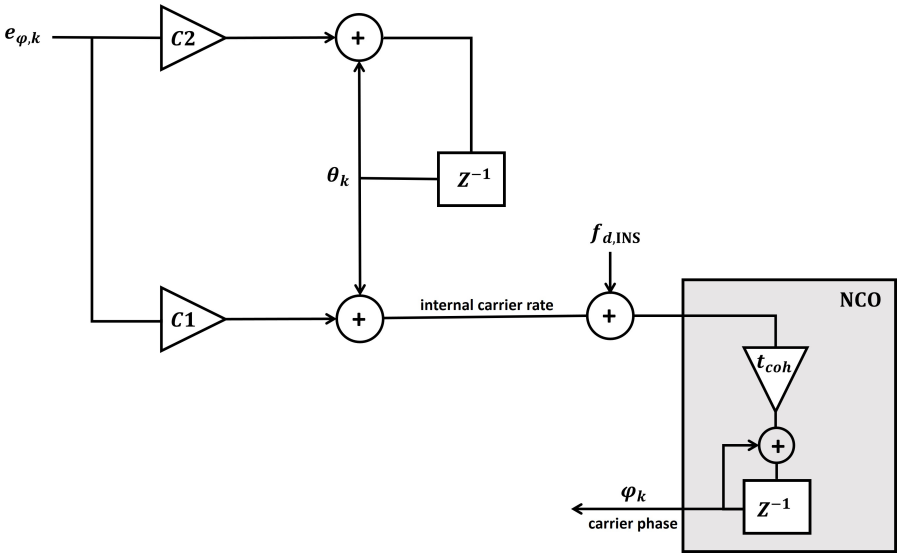

Figure 2: Block diagrams of the second order loop filters, adapted from Teunissen and Montenbruck (2017)

$$\begin{bmatrix} \varphi_{k+1} \\ \theta_{k+1} \end{bmatrix} = \begin{bmatrix} 1 & t_{coh} \\ 0 & 1 \end{bmatrix} \cdot \begin{bmatrix} \varphi_k \\ \theta_k \end{bmatrix} + \begin{bmatrix} C_1 \\ C_2 \end{bmatrix} \cdot e_{\varphi,k} + \begin{bmatrix} t_{coh} \\ 0 \end{bmatrix} \cdot f_{d,\text{INS}} \tag{4}$$

where $C_1 = \sqrt{2} t_{\text{coh}} \omega_0$, $C_2 = t_{\text{coh}} \omega_0^2$ and t_{coh} is the coherent integration time, which is in our case set to 5 ms, ω_0 is the natural frequency which can be derived from the PLL noise bandwidth B_{PLL} as $\omega_0 = 1.89 \cdot B_{PLL}$, $e_{\varphi,k}$ represents the carrier discriminator. The term θ_k represents the linear feedback shift register.

IV. DATA PROCESSING AND ANALYSIS

1. Experimental Setup

To investigate the impact of the external aiding of the receiver tracking loops, a measurement campaign under open sky conditions (see Fig. 3) has been conducted. As depicted in Fig. 4 the IFEN's SX3 front-end (2) was connected via a signal splitter to the Trimble Zephyr 2 geodetic antenna (1) to record intermediate frequency (IF) samples at 20 MHz. IMU data (accelerations and rotation rates) from the MEMS Xsens MTI-G-710 IMU (3) were also collected at a sampling rate of 200 Hz. In addition to that, as reference GNSS receiver, the Trimble NetR9 (4) was also connected to the same antenna realising a zero-baseline configuration with the SX3 front-end. To enable RTK carrier-phase positioning, a reference station with a Trimble NetR9 was running on top of the highest building of the campus (yellow triangle in Fig. 3) during the measurement campaign. The trajectory contains various movement scenarios, a static phase of 4 minutes at the beginning followed by 8-shape turns at approx. 40 km/h. For this contribution, only the first 2 minutes from the kinematic part of the trajectory were used to analyse and validate the concept of the high-quality PLL Doppler-aiding.

Figure 3: Left, car trajectory collected for the experiment. Right, skyplot of the GPS satellites available during the measurement campaign

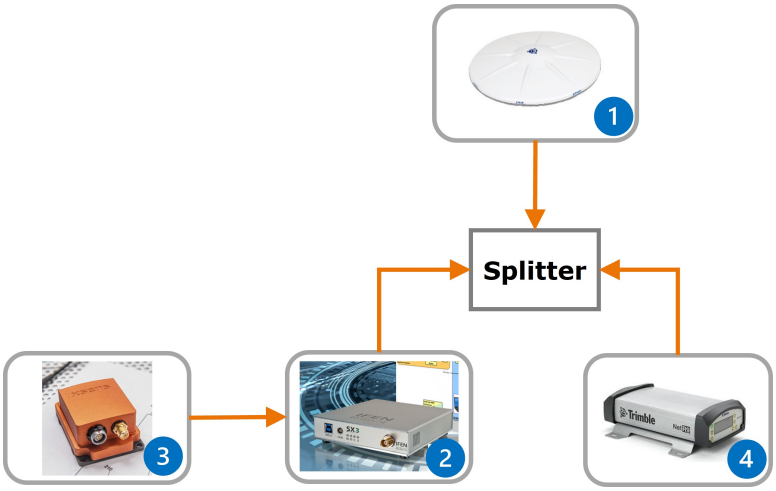

Figure 4: Experiment hardware setup employed for the car experiment

The characteristics of the MSRx receiver configuration are summarized in Tab. 1.

Table 1: Characteristics of the MSRx receiver

Parameter	Value
Signal Type	GPS L1 C/A
Radio Frequency	1575.42 MHz
t_{coh}	5 ms
PLL bandwidth	9 Hz
PLL order	2 (Costas)
DLL bandwidth	1 Hz
DLL order	2
Correlator spacing D	0.1 μsec
Measurement rate of GNSS receiver	1 s
Rate of sufficient statistic	0.5 s

2. Analysis of Aided and Unaided PLL Tracking Loops

For the analysis of the MSRx framework with Doppler aiding a dynamic interval of 45 seconds was selected. The trajectory covers the figure "eight" and is shown in Fig. 5 in the local east-north-up (ENU) coordinate frame. The right plot shows the RTK/INS (TrimbleNetR9-Xsens processed with NovAtel Inertial Explorer) high-rate reference trajectory in blue, the MSRx RTKLIB RTK solution (MSRx as a rover with a reference station) in yellow and the MSRx single point position (SPP) solution in red. The MSRx was configured for a Doppler aided PLL, where the Doppler values were derived from the reference trajectory (blue line). Therefore, the RTKLIB RTK and MSRx SPP solutions are based on the Doppler aided PLL.

The analysis shows a good but biased overlap of the MSRx RTKLIB RTK solution to the reference trajectory. This bias is currently under investigation. It it assumed, that it is caused by datum offsets. The MSRx SPP solution is significantly biased and the magnitude of the position bias is expected for a SPP L1 only solution without atmospheric corrections.

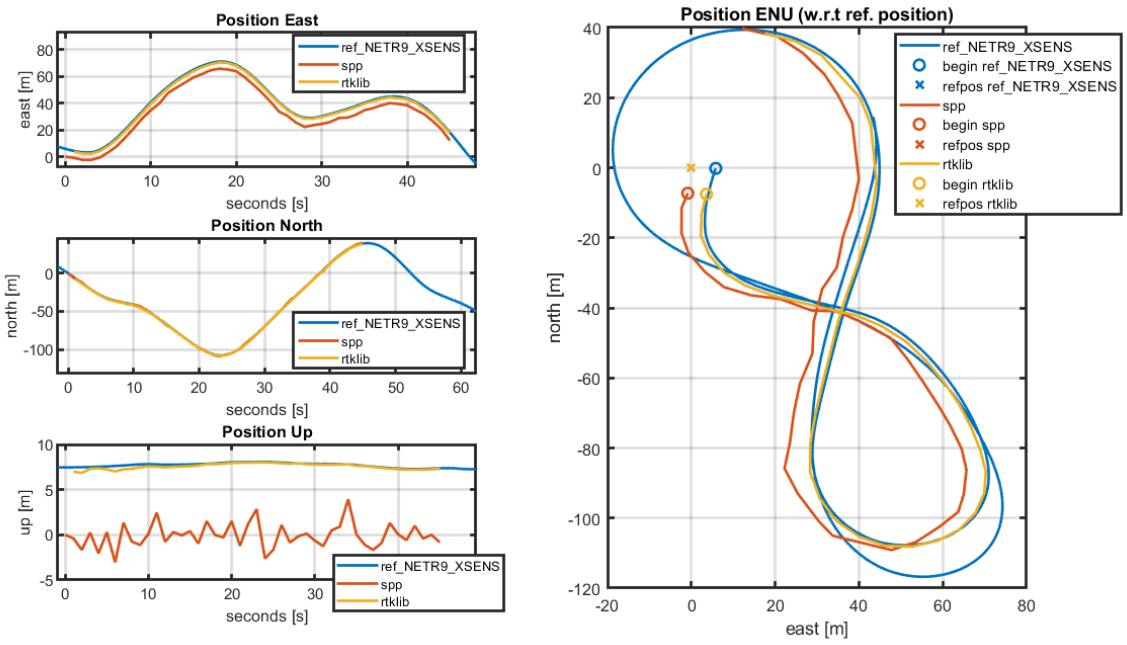

Figure 5: The plots show the selected interval for data analysis. The trajectory and position differences are shown in the local ENU coordinate frame. The figures on the left hand side show the position difference of the MSRx SPP and MSRx RTKLIB solution to the reference. The plot on the right shows the trajectories of all solutions. Hereby, the blue line is the RTK/INS reference trajectory, the yellow line is the RTKLIB RTK solution using the MSRx observations, and red is the MSRx SPP solution. The RTKLIB RTK and MSRx SPP solutions are generated using the Doppler aided PLL.

All loop parameters for the different setups are listed in Tab. 2 and apply for all shown plots, if not otherwise stated.

For the verification of the Doppler aided PLL, a comparison w.r.t. a conventional unaided PLL is shown in Fig. 6. The figures on the left refer to a conventional DLL/PLL loop with a PLL and the ones on the right correspond to a conventional DLL and a

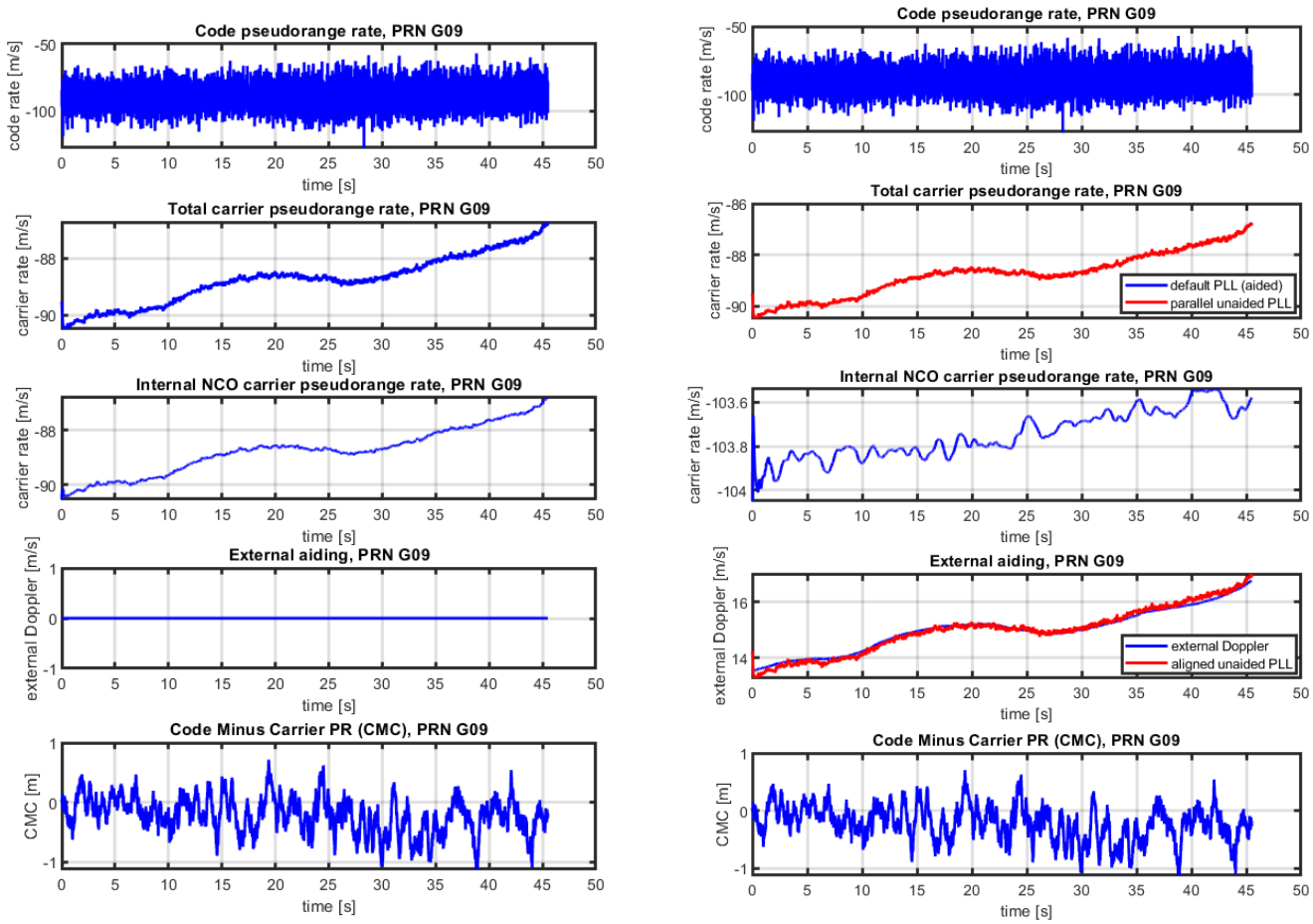

Figure 6: DLL/PLL tracking loop parameters. The left hand side shows the conventional DLL/PLL setup and the right hand side shows the conventional DLL and Doppler aided PLL setup. The red line refers to the PLL running in parallel, which is used for verification purposes like time synchronization.

Table 2: Default DLL/PLL loop settings of the MSRx receiver

	PLL BW	Loop order
Conventional DLL	1 Hz	2
Conventional PLL	9 Hz	2
Parallel unaided PLL	9 Hz	2

Doppler aided PLL. For the PLL three carrier rates are shown, the total carrier rate (used for generating the replica) which is split up into the external aiding component and remaining internal component such that

$$\dot{\varphi}_{\text{total}} = \dot{\varphi}_{\text{internal}} + \dot{\varphi}_{\text{external}} \tag{5}$$

where $\dot{\varphi}$ refers to the carrier pseudorange rate. Thus, for the conventional DLL/PLL setup the external aiding component $\dot{\varphi}_{\text{external}} = 0$ and $\dot{\varphi}_{\text{total}} = \dot{\varphi}_{\text{external}}$. For the Doppler aided loop the external loop component from the RTK/INS reference solution covers the receiving antenna motion and consequently represents the carrier rate in LOS direction. The carrier phase model from (Teunissen and Montenbruck, 2017, eq. 14.79) and carrier Doppler from (Teunissen and Montenbruck, 2017, eq. 14.82) shall support the understanding of the plots and are defined as

$$\varphi = \lambda N + \rho - c(dt_r - dt^s) - I + T + c(\delta_r + \delta^s) + p_T + \epsilon_{mp} + \epsilon_n \tag{6}$$

$$\dot{\varphi} = f_d = -\frac{1}{\lambda}[\dot{\rho} - c(\dot{dt}_r - \dot{dt}_s) + p'_T + \epsilon'_{mp} + \epsilon'_n] \tag{7}$$

where N is the carrier ambiguity, c is the speed of light, dt_r and dt^s are the receiver and satellite clock errors, I and T are the ionospheric and tropospheric delays, p_T are transient errors, ϵ_{mp} multipath errors and ϵ_n noise. Equation (7) represents the first derivative of (6), whereas atmospheric error sources (ionosphere and troposphere) change slowly in time and therefore are neglected. Furthermore it should be noted, that the carrier phase windup is not considered in the equations. These equations should help to interpret the plots. In case of a Doppler aided PLL, the components in (5) can be modeled as

$$\dot{\varphi}_{\text{total}} = \dot{\varphi} \tag{8}$$

$$\dot{\varphi}_{\text{external}} = -\frac{1}{\lambda}\dot{\rho} = f_{d,\text{INS}} = f_{d,\text{true}} + \frac{1}{\lambda}\epsilon_{\text{INS}} \tag{9}$$

$$\dot{\varphi}_{\text{internal}} = \frac{1}{\lambda}[c(\dot{dt}_r - \dot{dt}_s) - p'_T(\epsilon_{\text{INS}}) - \epsilon'_{mp} - \epsilon'_n - \epsilon_{\text{INS}}] \tag{10}$$

where ϵ_{INS} is the aiding error, which depends on the quality of the used IMU and the duration of GNSS outages (in case of a GNSS/INS system for the external aiding). The symbol $f_{d,\text{true}}$ represents the true LOS Doppler.

The aiding error ϵ_{INS} cancels in (5), but it is very important to note that the NCO has to follow it and thus the transient error $p'_T(\epsilon_{\text{INS}})$ depends on it. For low PLL loop bandwidths, the quality of the IMU incl. the strapdown computation and error model has to be reasonable high sucht that $f_{d,\text{INS}}$ accurately follows the LOS dynamics.

The components from (5) - (10) are visualized in Fig. 6 by the second, third and fourth plot. The third plot of the internal carrier pseudorange rate in case of Doppler aiding is of interest, as it covers the receiver clock drift, the satellite clock drift, transient errors, multipath errors and noise. Here, a valid time synchronisation between GNSS and INS is essential. In order to visualize synchronization errors, a second unaided PLL was operated in parallel, which captures the full carrier pseudorange and pseudorange-rate. Based on the fact, that the antenna motion component is dominant in case of a dynamic scenario, the signature of the resulting pseudorange-rate must fit to the external aiding component. Therefore, the pseudorange-rate of the unaided parallel PLL was plotted in red against the total carrier pseudorange rate and external aiding component. It can be seen that the signatures fit exactly, so that proper time synchronisation can be assumed.

The internal carrier pseudorange-rate as defined in Eq.(10) contains a component common for all satellites, the receiver clock drift $c\,\dot{dt}_r$. This common and typically dominant component can be seen very prominently in Fig. 7. The plot shows also a simple receiver clock drift estimate using the epoch-wise mean of all satellites by the yellow line. For visualization purposes the aided PLL loop bandwidth was increased to 9 Hz, such that the aided loop follows the components in (10) quickly.

The analysis of both code and carrier discriminators is shown in Fig. 8. The plot on the left shows the conventional DLL/PLL setup and the ones on the right refer to the conventional DLL with Doppler aided PLL. Both setups show DLL results as expected

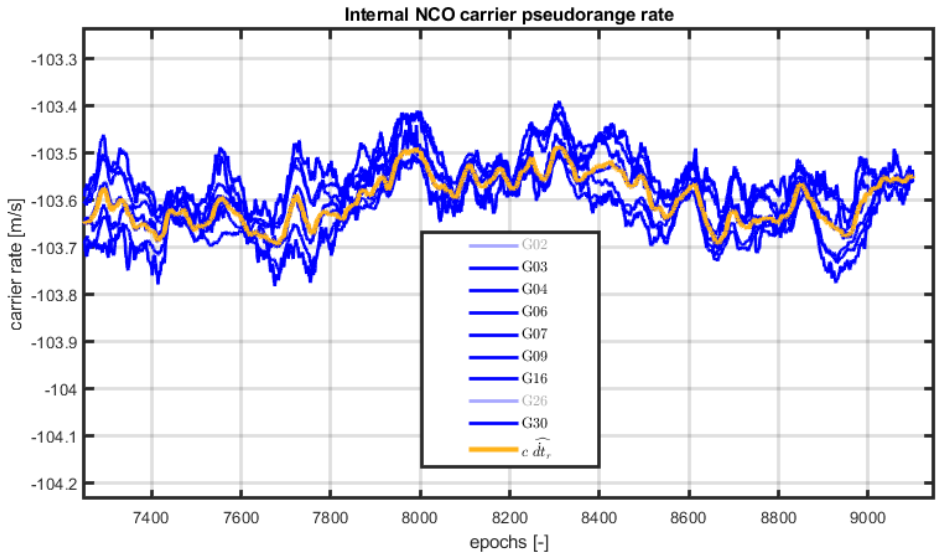

Figure 7: Overlap of representative satellites to visualize the common receiver clock drift. PRN02 and PRN26 have been excluded because they have large multipath variations and thus high deviations from the clock error, which makes the common signature less visible. A simple clock drift estimate using the epoch-wise mean of all satellites is shown by the yellow line.

with a code noise of about $\sigma_{\Delta\tau} = 3.2$ m, which is typical for good GPS L1 signal reception and the current configuration. The carrier discriminator of the conventional setup shows a $\sigma_{\Delta\varphi} = 0.01$ cyc, which also meets the expectations. The carrier discriminator of the aided PLL is of higher interest. Due to the Doppler aiding as defined in (9), the carrier range component in (6) is also aided because of $\rho = \int \dot{\rho}\, dt$. The aided PLL was initialized 2 sec after startup from the converged conventional PLL. Furthermore, due to the small aided PLL loop bandwidth of 2 Hz, the carrier NCO reluctantly follows the remaining components in (6). Some remaining components can be seen nicely by the fluctuations in the bottom right plot of Fig. 8. Based on the fact that the satellite clock error (high grade atomic clock), the ionosphere and troposphere change slowly in time, the dominant part of the fluctuations are caused by the receiver clock error, transient errors, multipath, noise and the aiding error.

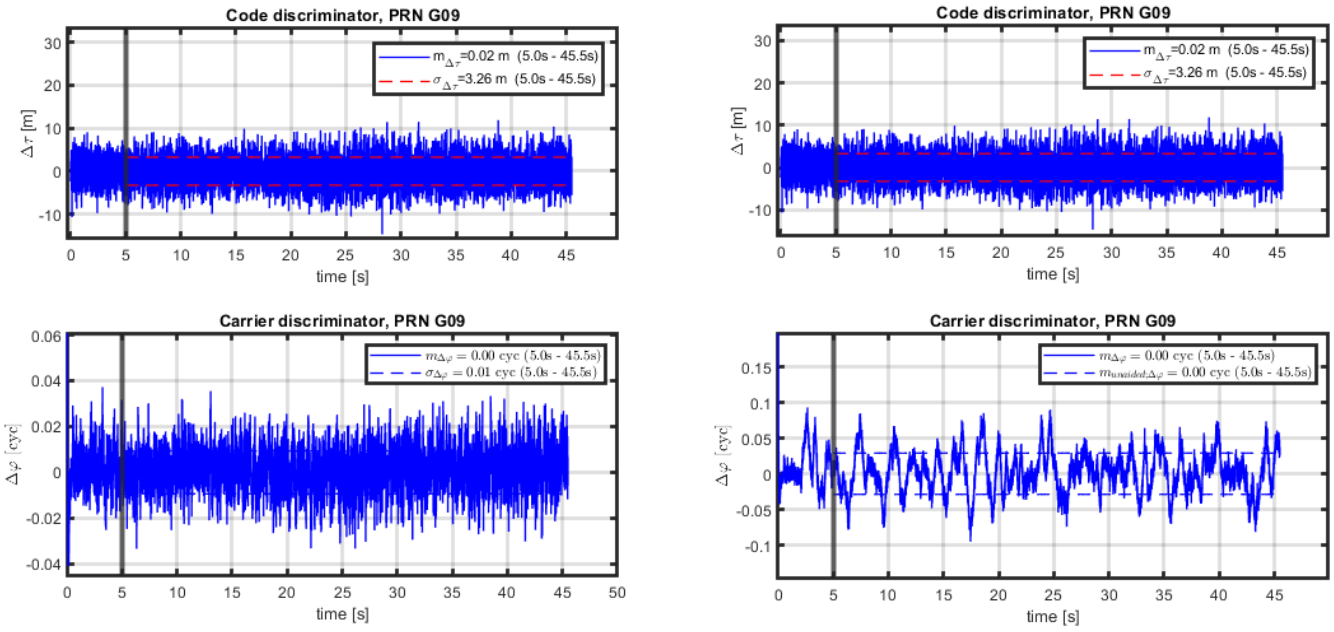

Figure 8: Code and carrier discriminator. The left plots show the conventional DLL/PLL setup, the right plots show the conventional DLL with Doppler aided PLL. The red line shows the unaided parallel PLL as reference.

The common receiver clock error can be seen by the common discriminator signature as shown in the upper plot of Fig. 9. The yellow line shows a simple (relative) clock error estimate by calculating the epoch-wise mean of the discriminator value of all satellites. After removing the clock error signature, the dominant remaining components is the carrier multipath, which was also the reason for selecting the stronger multipath affected satellite PRN02.

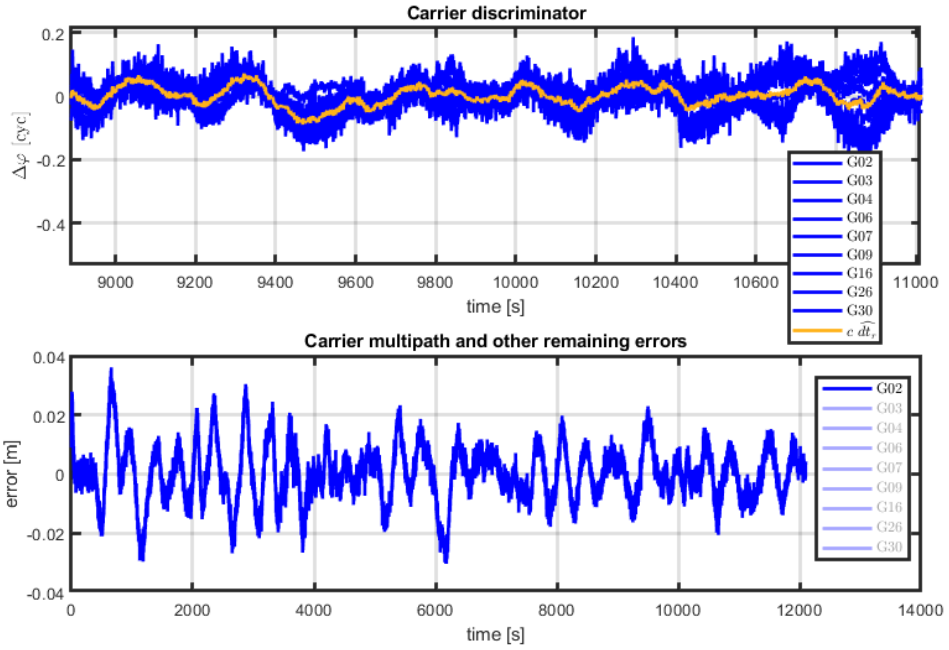

Figure 9: The upper plot shows the discriminators of all satellites in blue and the common receiver clock error estimate using a epoch-wise mean of all satellites in yellow. The lower plot shows the remaining errors of PRN02 when removing the receiver clock error estimate from the discriminator value. The most dominant remaining error is carrier multipath, where for visualization purposes PRN02 was selected for display.

3. RTK Results with Doppler-Aided PLL

The RTK results have been achieved by post-processing the MSRx receiver independent exchange format (RINEX) output files together with the RINEX of the reference station using the RTKLIB open source software package. The distance to the Trimble NetR9 reference receiver was about 400m to achieve a short baseline and a good fixing rate with GPS L1 only. The results are shown in Fig. 10. The analyzed interval is 120 seconds. The achieved fixing rate is about 80 percent, mostly resulting from an initial convergence phase of the RTKLIB. When comparing the results in Tab. 3, the Doppler-aided PLL with $B_{\text{PLL,aided}} = 2$ Hz is performing slightly worse. As shown in Fig. 7 and Fig. 9, the PLL is not following the receiver clock error and drift properly. This improper tracking of carrier-range and range-rate components causes a reduced fixing rate of the RTKLIB. A verification with a higher PLL loop bandwidth of $B_{\text{PLL,aided}} = 5$ Hz to cover the receiver clock error and drift already shows slightly better results compared to the conventional PLL. Thus it is expected that the usage of the CoOp-tracking method will allow further reduction of the loop bandwidth. The CO-OP tracking method allows to track the receiver clock parameters independently with a high loop bandwidth of e.g. $B_{\text{PLL,CO-OP}} = 9$ Hz, while the remaining components can be tracked with a low bandwidth e.g. $B_{\text{PLL,aided}} = 0.2 - 2$ Hz.

Table 3: RTK fixing rates for a conventional and Doppler aided PLL with different loop bandwidths

	PLL BW	RTK fix rate
Conventional PLL	9 Hz	80.3 %
Doppler-aided PLL	2 Hz	68.1 %
Doppler-aided PLL	5 Hz	80.5 %

V. TOWARDS SYNTHETIC APERTURE PROCESSING WITH AN INS-AIDED PLL

When performing Doppler-aiding of a PLL with an INS, the short term motion of the antenna is captured to a large extent by the inertial sensor. This concept is very similar to SAP, where correlation values are projected onto the LOS motion in order to purify the correlation values from multipath (i.e. beamforming in LOS-direction). For SAP this is done for a so called beamforming

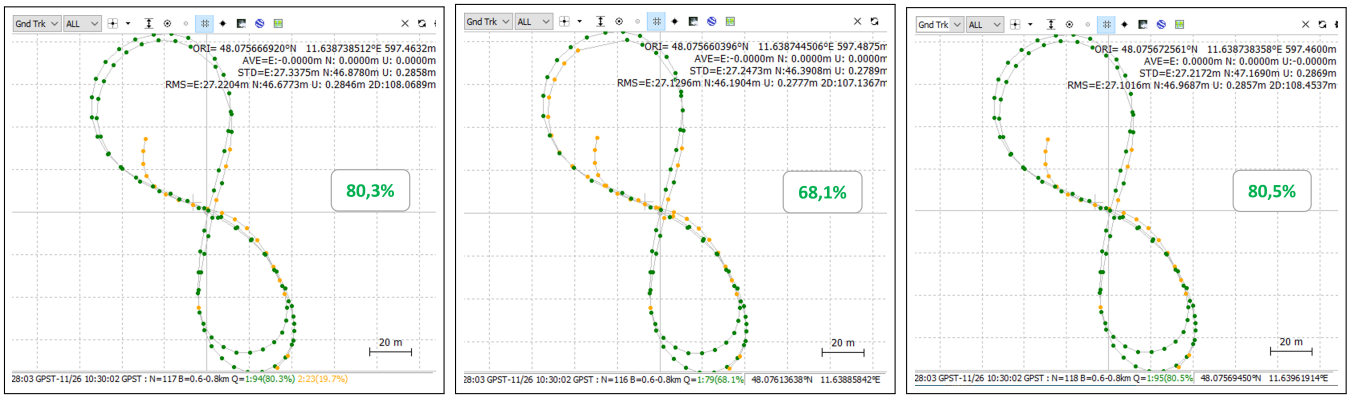

Figure 10: RTK results from RTKLIB. From left to right: the conventional PLL with $B_{\text{PLL}} = 2$ Hz, the Doppler-aided PLL with $B_{\text{PLL,aided}} = 2$ Hz and $B_{\text{PLL,aided}} = 5$ Hz

interval T_{BF}. The spatial motion of the antenna within this interval of typically 1-2 sec (Pany et al., 2013; Dampf et al., 2016, 2017) is used to generate a synthetic antenna aperture to suppress signals from unwanted direction of arrivals (DOAs). There are two major differences between full SAP and and a Doppler aided PLL:

1. The aided PLL still follows the true GNSS carrier pseudorange to some extend according to the defined aided PLL loop bandwidth e.g. $B_{\text{PLL,aided}} = 0.2 \ldots 2$ Hz
2. For a Doppler aided PLL the effective beamforming interval could be defined as $T_{\text{BF,aided}} = \frac{1}{B_{\text{PLL,aided}}}$, with $t_{\text{coh,aided}} << T_{\text{BF,aided}}$ [coherently summing up all integrate and dump (I&D) batches of shorter duration $t_{\text{coh,aided}} = 5 \ldots 20$ ms].

This means that a Doppler aided PLL using an INS implicitly observes an SAP effect, even if the effect is not that large. The quantification of SAP with a Doppler aided PLL is planned for further research. The method of a Doppler or carrier-phase aided PLL for SAP has the benefit, that it can be realized as a continuous and integral part of a tracking loop, whereas the work in (Pany et al., 2013; Dampf et al., 2016, 2017) follows a batch processing approach.

VI. OUTLOOK

The way forward will be the realization of a carrier-range aided PLL based on the precise and high-rate RTK/INS reference solution. Hereby, Fig. 11 shows the current status (left) and the next realization step (right). As shown in the right block diagram, the estimated carrier phase will be injected into the tracking loop after the integration step of the NCO. Additionally it ts planned to estimate the receiver clock error using a CO-OP-tracking loop, which is a combined tracking loop over all channels. The clock tracking loop uses the prompt correlation values P_i of each channel as input. The prompt-correlation values from the I&D epochs need to be synchronized in time before calculating the discriminator. The clock tracking loop bandwidth will be adjusted to the used clock type e.g. TCXO or OCXO. The estimated clock error will be added to the carrier phase estimate, before generating the carrier replica. After this step, the resulting dominant component on the carrier discriminators will just be multipath.

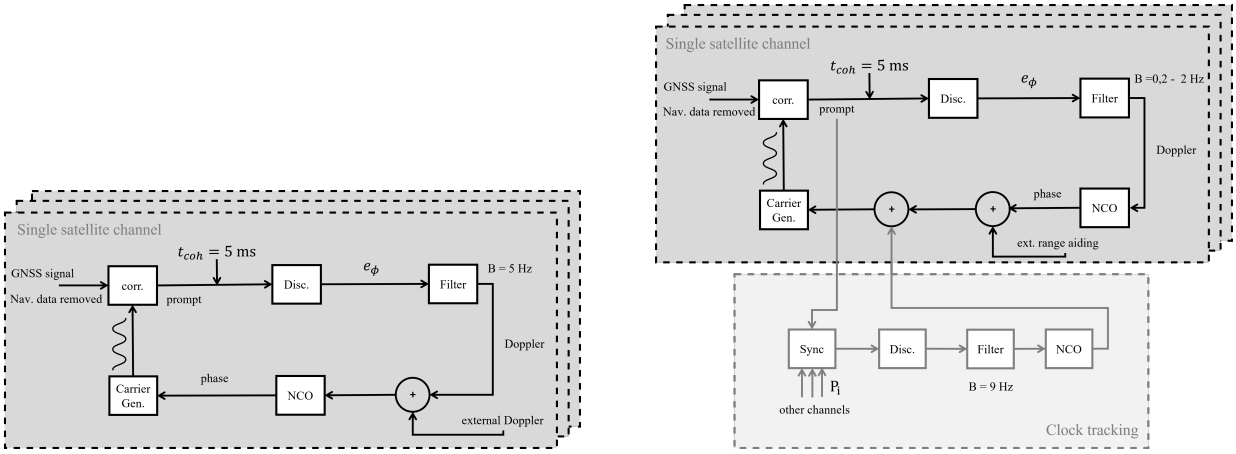

Figure 11: The figure on the left shows the current status with a Doppler-aided PLL. The figure on the right shows the next step, a carrier-range aided PLL with CO-OP-tracking to estimate the receiver clock.

Mitigating the multipath with SAP requires a further adaption step in addition to the carrier range aiding as shown in Fig. 12. Hereby, SAP uses an additional beamforming step which coherently accumulates the correlation values (e.g. coherent batches of $t_{\text{coh}} = 5\,\text{ms}$ from the correlator. The accumulation interval is defined by the beamforming interval, e.g. $T_{\text{BF}} = 1\,\text{s}$. In order to build the coherent sum, the navigation data bits need to be removed from the correlation values. The sum contains a complex weighting factor w_i for each correlation value i, which can be used to realize different beam-steering strategies. For SAP the antenna motion and clock error on the carrier-phase is already tracked, thus the PLL bandwidth of the carrier-loop filter can be reduced to e.g. $B = 0,2\,\text{Hz}$.

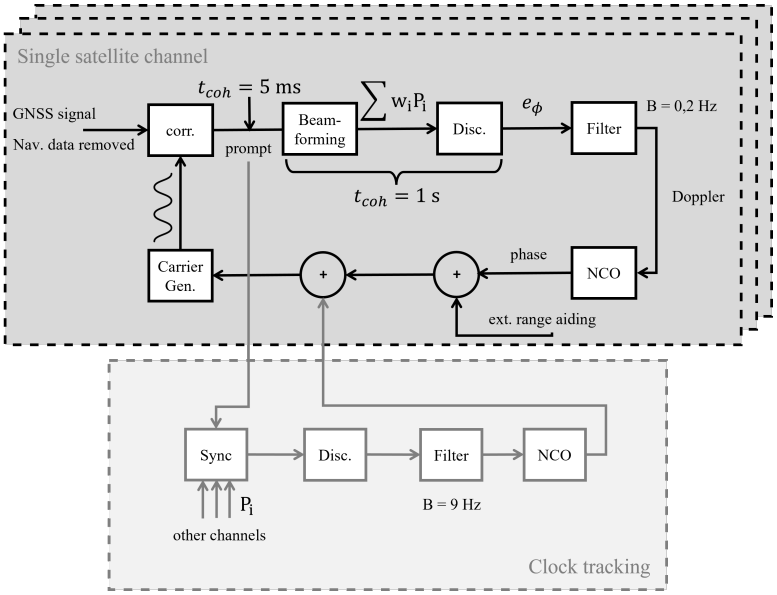

Figure 12: Concept of synthetic aperture processing with an additional beamforming block after retrieving the correlation values from the correlator. The beamforming block coherently accumulates correlation values up to a defined beamforming interval.

VII. CONCLUSION

This work summarizes the current status of the development of a high-end MATLAB based analysis platform for SAP. The presented status is a Doppler-aided PLL with a high-quality RTK/INS trajectory with outstanding capabilities, which is the innovative and unique part. The achieved results with the Doppler-aided PLL, the simplest form of SAP have been compared to a standard PLL in the context of tracking performance, positioning performance, RTK and SAP. The way forward to realize a carrier-range aided PLL, CO-OP-tracking to estimate the receiver clock and implement long-coherent beamforming as integral part of the tracking loop is discussed in detail.

ACKNOWLEDGEMENTS

The results presented in this work were developed within the project *"Forschungs- und Studienvorhaben für Innovationen des Galileo GNSS-Systems (GalileoFusion)"* funded by the German Federal Ministry for Economic Affairs and Energy (BMWi) and administered by the Project Management Agency for Aeronautics Research of the German Space Agency (DLR) in Bonn, Germany (grant no. 50NA2001). Any opinions, findings, conclusions, or recommendations expressed in this material are those of the author and do not necessarily reflect the views of UniBw M nor DLR.

REFERENCES

Alban, S., Akos, D. M., and Rock, S. M. (2003). Performance analysis and architectures for INS-aided GPS tracking loops. In *Proceedings of the 2003 National Technical Meeting of The Institute of Navigation*, pages 611–622.

Bochkati, M., Dampf, J., and Pany, T. (2022). On the Use of Multi-correlator Values as Sufficient Statistics as Basis for Flexible Ultra-tight GNSS/INS Integration Developments. In *2022 25th International Conference on Information Fusion (FUSION)*, pages 1–8.

Dampf, J., Pany, T., Bär, W., Mervart, L., Rodriguez, J.-A., and Ioannides, R. (2017). Real World Spoofing Trials and Mitigation via Direction of Arrival Discrimination. *Inside GNSS*, May/June 2017:20–30.

Dampf, J., Pany, T., Bär, W., Winkel, J., Stöber, C., Mervart, L., Rodriguez, J. A., and Ioannides, R. (2016). Real World Direction

of Arrival Estimation and Mitigation of Spoofing Signals with a Synthetic Aperture Antenna. In *Proceedings of the Navitec 2016*. ESA-ESTEC.

EUSPA (2022). *EUSPA EO and GNSS Market Report.2022 / Issue 1* . Publications Office of the European Union.

Faragher, R., Couronneau, N., Powe, M., Esteves, P., Crocket, M., Martin, H., Ziglioli, E., Higgins, C., and Buckle, D. (2018). Supercorrelation: Enhancing the Accuracy and Sensitivity of Consumer GNSS Receivers with a DSP Upgrade. In *Proceedings of the 31st International Technical Meeting of the Satellite Division of The Institute of Navigation (ION GNSS+ 2018)*, pages 357–375, Miami, Florida.

Gao, G. and Lachapelle, G. (2008). A Novel Architecture for Ultra-Tight HSGPS-INS Integration. *Positioning*, 1(13).

Gebre-Egziabher, D., Razavi, A., Enge, P., Gautier, J., Pullen, S., Pervan, B., and Akos, D. (2005). Sensitivity and Performance Analysis of Doppler-Aided GPS Carrier-Tracking Loops. *Navigation*, 52:49–60.

Kaplan, E. D. and Hegarty, C. J. (2017). *Understanding GPS/GNSS: Principles and Applications*. GNSS Technology and Applications Series. Artech House, Boston and London, third edition.

Kay, S. M. (1993). *Fundamentals of Statistical Signal Processing: Estimation Theory*, volume I of *Fundamentals of Statistical Signal Processing*. Prentice Hall.

NovAtel Inc. (2018). Inertial Explorer 8.70 User Manual.

Pany, T., Dötterböck, D., Gomez-Martinez, H., Hammed, M. S., Hörkner, F., Kraus, T., Maier, D., Sanchez-Morales, D., Schütz, A., Klima, P., and Ebert, D. (2019). The Multi-Sensor Navigation Analysis Tool (MuSNAT) – Architecture, LiDAR, GPU/CPU GNSS Signal Processing. In *Proceedings of the 32nd International Technical Meeting of the Satellite Division of The Institute of Navigation (ION GNSS+ 2019)*. Institute of Navigation.

Pany, T. and Eissfeller, B. (2006). Use of a Vector Delay Lock Loop Receiver for GNSS Signal Power Analysis in Bad Signal conditions. In *Proceedings of IEEE/ION PLANS 2006*, pages 893–903.

Pany, T., Falk, N., Riedl, B., Stöber, C., and Winkel, J. (2013). GNSS Synthetic Aperture Processing with Artificial Antenna Motion. In *Proceedings of the 26th International Technical Meeting of the Satellite Division of The Institute of Navigation (ION GNSS+ 2013)*, ION GNSS+, The International Technical Meeting of the Satellite Division of The Institute of Navigation. Institute of Navigation.

Rothacher, M. and Beyerle, G. (2008). GPS C/A Navigation Message Data Bits. doi:10.1594/GFZ.ISDC.GNSS/GNSS-GPS-1-NAVBIT.

Sharma, H., Bochkati, M., Lichtenberger, C. A., Pany, T., Darguna, F., and Wübbena, J. B. (2021). Smartphone-based GNSS Positioning – Today and Tomorrow. *Inside GNSS*.

Spilker Jr., J. J., Parkinson, S. U. J. S. B., and Parkinson, B. W. (1996). *Global Positioning System: Theory and Applications, Volume II*. AIAA.

Suzuki, T. and Kubo, N. (2014). GNSS-SDRLIB: An Open-Source and Real-Time GNSS Software Defined Radio Library. In *Proceedings of the 27th International Technical Meeting of the Satellite Division of The Institute of Navigation (ION GNSS+ 2014)*, pages 1364–1375.

Teunissen, P. J. G. and Montenbruck, O. (2017). *Springer Handbook of Global Navigation Satellite Systems*. Springer, Cham, Switzerland.

Tsujii, T., Fujiwara, T., Suganuma, Y., Tomita, H., and Petrovski, I. (2011). Development of INS-Aided GPS Tracking Loop and Flight Test Evaluation. *SICE Journal of Control, Measurement, and System Integration*, 4(1):15–21.

Zhang, T., Ban, Y., Niu, X., Guo, W., and Liu, J. (2017). Improving the Design of MEMS INS-Aided PLLs for GNSS Carrier Phase Measurement under High Dynamics. *Micromachines*, 8(5):135.